Carpio, P.; Rayón Encinas, E.; Pawlowski, L.; Cattini, A.; Benavente Martínez, R.; Bannier, E.; Salvador Moya, MD.... (2013). Microstructure and indentation mechanical properties of YSZ nanostructured coatings obtained by suspension plasma spraying. Surface and Coatings Technology. 220:237-243. doi:10.1016/j.surfcoat.2012.09.047.

Microstructure and Indentation Mechanical Properties of YSZ Nanostructured Coatings Obtained By Suspension Plasma Spraying

P. Carpio[1,*], E. Bannier[1], L. Pawlowski[2], R. Benavente[3], E. Rayón[3], M.D. Salvador[3,], E. Sánchez[1]

[1] Instituto de Tecnología Cerámica (ITC). Universitat Jaume I. Castellón, Spain

[2] Science des Procédés Céramiques et de Traitements de Surface (SPCTS, UMR CNRS 6638). Université de Limoges. Limoges, France

[3] Instituto de Tecnología de Materiales (ITM). Universidad Politécnica de Valencia. Valencia, Spain.

Abstract

A commercial nanosuspension of yttria-stabilized zirconia (YSZ) was successfully deposited on austenitic stainless steel substrate by suspension plasma spraying technique (SPS). A SG-100 torch with internal radial injection was used for the spraying and a pneumatic system transported the feed suspension from the containers to the injector. In order to study the effect of the spraying parameters, a factorial model was used to design the experiments, changing both spraying translation speed and suspension flow rate.

The coating microstructure was characterised by FEG-SEM. All coatings displayed a bi-modal microstructure formed by nanometre-size particles surrounded by fully molten areas. Moreover, crystalline phases were determined by XRD and Raman spectroscopy. Mechanical properties were also determinated using nanoindentation technique. Nanoindentation tests confirmed a bimodal distribution of the mechanical properties (hardness and Young's modulus) which related to the two zones (molten and partially molten) present throughout the coatings.

Introduction

Nanostructured coatings have been extensively studied in the last decade and thermal spraying is one of the techniques commonly used to obtain such layers. In fact, coatings which exhibit different architectures and enhanced properties can be obtained by using nanostructured feedstock in plasma spraying. In the case of YSZ coatings for thermal barriers, nanostructured coatings can offer better performance than that of their conventional counterparts as reported elsewhere [1, 2]. In particular, literature shows that the non-molten nanostructured zones present in YSZ coatings obtanining by APS decrease the thermal conductivity and increase the thermal shock resistance of the thermal barriers [3]. However, nanoparticles cannot be injected directly in the plume, due to their low density and poor flowability [4]. One possible solution is using a carrier liquid and inject a suspension of nanoparticles inside the plasma plume instead of a powder. This process is known as suspension plasma spraying (SPS) [5].

Previous research has shown that TBCs obtained by SPS exhibit lower thermal conductivity and higher thermal shock resistance without substantially varying the hardness or elastic modulus due to higher segmentation crack densities[6]. However, the deposition ratio of SPS technique is much less than that of conventional APS technique. This makes it difficult to obtain thick coatings. Thickness of SPS coatings typically ranges from 30 to 70 μm. As a consequence of the low thickness of the SPS coatings, it was found that nanoindentation technique is a more feasible method than conventional microindentation for the mechanical characterisation of such layers.

Much research work about the characterization of the mechanical properties of materials by using the nanoindentation technique has been published in the last years. However, the amount of papers dealing with the use of nanoindentation method to characterize SPS layers is much more scarce [7, 8]. Wang et al. [9] have investigated YSZ coatings

obtained from APS, nanostructured powder. The coatings showed a bimodal microstructure made up of molten and partially molten zones meanwhile each of these zones exhibited different hardness and elastic modulus. Lugsheider et al. [10, 11] conclude that the mechanical properties in vertical and horizontal directions are different for TBCs obtained by EB-PVD. Gross and Saber-Samandari [12] studied hydroxyapatite coatings obtained by SPS, concluding that, despite being more porous coatings that those obtained by conventional APS, the overall coating hardness was also similar because the hardness of non-porous areas was also very high. Finally, the authors of this research have recently reported some works on the use of nanoindentation technique for mechanical characterisation of APS and SPS coatings. In a first paper [13], the crystalline phases anatase and rutile were identified in SPS TiO_2 coatings by nanoindentation technique on the basis of the difference in Young's modulus of these two phases. Similarly, in WC-Co coatings obtained by APS carbide phases with different hardness values were successfully identified [7].

In this work, a commercial suspension of YSZ nanoparticles was deposited by SPS. In order to address the effect of the spraying parameters, a factorial model was used to design the experiments, meanwhile the effect of both spraying translation speed and injection pressure were considered. Finally, coatings were also microstructurally and mechanically characterised, and the influence of the spraying parameters on microstructure and mechanical properties was evaluated. The mechanical properties were determined by means of a nanoindentador.

Experimental techniques

Materials

A commercial aqueous suspension of 3 mol% yttria-stabilized zirconia (YSZ) nanoparticles (MELox Nanosize 3y, Mel Chemicals, United Kingdom) was used as

feedstock. According to the information provided by the supplier, particles specific surface area is 85-96 m^2/g and particle average size is 11-12 nm. Suspension solid content is approximately 5 vol.%.

TEM observations (H710, Hitachi, Japan) of the nanoparticles in this suspension confirmed their nanometre size (10-20 nm). XRD analysis (D5000, Siemens, Germany) indicated that it only contains tetragonal phase.

AISI 304 stainless steel specimens in the form of 25 mm diameter and 10 mm thickness disks were used as substrates. Before deposition, the substrates were grit blasted with corundum and cleaned with acetone in an ultrasounds bath.

Coating deposition

All coatings were sprayed using an internal radial injection torch (SG-100, Praxair, USA). This torch was adapted for SPS and a pneumatic system was used to transport the liquid to the injector. This system consists of two pressurized containers so that the liquid inside them is forced to flow to the injector. This device had a 150 μm diameter hole and it was connected to the plasma gun. A filter was used to remove agglomerates of nanoparticles and probable contaminations. Suspension feeder rate was controlled by adjusting the pressure in the suspension containers. Samples were mounted on a rotating device and up to 6 samples were coated simultaneously.

The main spraying parameters used for each sample, as well as for the reference sample, are given in table 1. In this work, full factorial design of experiments 2^k with a middle point [14] was used in order to study the influence of the parameters on the coating microstructure and properties. In this case, two parameters were varied (injection pressure and spraying linear speed) and two levels for each parameter were considered. Moreover, a middle point was established where the parameters were set to the average value of the other two levels. The midpoint was chosen from previous work experience

[15]. Cooling was performed with compressed air (4 bar). During deposition, the temperature of the samples was measured using a pyrometer (In 5 Plus, Impac, France). After 3 spraying passes, the deposition was stopped and samples were cooled until 80 ºC. The required number of spraying cycles were used to obtain coatings of 30 µm thickness.

Coating characterisation

Coatings surface and cross-section were observed by field emission scanning electron microscopy (FEG-SEM, S-4800, Hitachi, Japan) in order to microstructurally characterise them. For the purpose of observing the cross-section, the samples were embedded in epoxy-resin and polished. In addition, X-ray diffraction patterns of the coatings were collected using the diffractometer D5000 (Siemens, detector Sol-XDet, CuKα 1.5406 Å, operating at 40 kV - 30 mA). Besides, a HORIBA Jobin Yvon Raman spectrometer configured at 514.5 nm emission was used to characterise some of the coated sample cross-sections. The localisation of the analysis spot of the argon-ion laser was driven by an optical microscope.

The nanoindentation tests were performed by a G-200 nanoindenter from Agilent Technologies using a previously calibrated diamond Berkovich tip on silica reference material. The stiffness was calculated by a Continuous Stiffness Measurement mode set at 2 nm harmonic oscillation amplitude and at 45 Hz oscillation frequency. The location of tests was guided by an optical microscope included in the nanoindenter machine. Indentations were performed on the polished sample at the cross-sectional view and at a constant 2000 µm depth. Details of this method were reported [7, 13].

Results and discussion

Spraying parameters influence the maximum temperature reached by the coatings during the deposition (Table 1). On the one hand, when the linear speed is increased,

maximum temperature decreases because of a shorter spraying time. On the other hand, when the injection pressure is increased, maximum temperature also decreases. Actually, the feed suspension flow rate grows at higher pressure, so a greater part of the plasma enthalpy is necessary to evaporate the solvent.

The cross-sectional SEM images of the as-sprayed coatings revealed two well differentiated microstructures, named as (*I*) molten and (*II*) non molten areas (Figure 1). Thus, the revealed bimodal structure is caused by the temperature heterogeneities reached in the plume. Some of the YSZ powder was molten forming great drops in fly, while a great quantity of fine powder reached the substrate without melting. The characteristic splat microstructure, more typical of the coatings produced by APS technology but also found in some SPS coatings [16], was visible in zones where the molten drops impacted on a previously deposited molten area. Nevertheless, the fine powder was deposited and sintered forming the matrix microstructure. This fine particle microstructure contains several cracks growing respect to the normal of the substrate, referred as *N-cracks*. The *N-cracks* achieve the entire thickness of the unmolten particles microstructure and it seems that the neighbour molten areas served as cracking barrier zones. This type of cracks are evidencing stresses stored in the coating probably due to differences of the volumetric expansion of the system substrate/TGO/coating and by the temperature gradients generated along the spraying process. However, several cracks grow parallel to the substrate (*P-cracks*) at the molten grain boundaries, indicating poor cohesion. The *P-cracks* are the most undesired faults because it can induce delaminate failure [17,18].

The cross-section of all coatings is shown in figure 2 and the surface in figure 3. Among all the obtained coatings, little difference can be found in the cross-section (Figure 2) and surface (Figure 3) micrographs. When the injection pressure was high, and

consequently feed suspension flow rate increased, the melting grade decreases because a higher part of the plasma enthalpy is used to evaporate the solvent. On the other hand, the samples 2 and 3 seem to display a more homogeneous microstructure (Mr. Pawlowski, could you give an explanation for it?

The XRD patterns of all coatings only show the presence of tetragonal phase (Figure 4). It is the usual phase in as-sprayed coatings when the yttria proportion is 3 mol%, since the goal of the doping is to stabilize tetragonal phase at room temperatures. [19]. Further microprobe Raman analysis corroborated the DRX results set out above, indicating that both microstructures (unmolten and molten) correspond to the same tetragonal phase.

As previously mentioned above the use of the nanoindentation technique is justified by the thin thickness of the coatings, being unworkable the employment of other standardized microhardness techniques. Although the microstructure produces an undesirable effective roughness for nanoindentation analysis, tests were carefully executed on individual flat microstructures assuring the minimum possible roughness effect. Locations were then chosen on the molten areas (*I*) and on the fine microstructure (*II*), as figure 5 shows. Furthermore, several indentations were performed on locations with a mixture of both microstructures (*I*+*II*).

Figure 6 and figure 7 show the hardness and elastic modulus obtained for each microstructure tested, respectively. Below 1 μm depth a great dispersion of values is justified by the roughness and by the heterogeneity of microstructures beyond the indenter. Even so, three tendencies were clearly observed in depth for *H* and *E* curves. Hardness results acquired for the big molten areas *(I)* at the experimented load interval ranged from 8 GPa to 12 GPa, while hardness in the matrix of fine particles *(II)* was stabilized at 2 GPa. The indentations which achieved mixture of microstructures

showed hardness values stabilized on 4 GPa as expected by the mixture law. The *E* and *H* value agree with the reported tendency in nanostructured APS YSZ coatings [9] and nanostructured YSZ coatings obtained by SPS [8]. With regard to elastic modulus findings, the obtained values ranged from 125 to 150 GPa. for molten areas and 65 GPa for the matrix. However no paper was found that reports a bimodal distribution of nanoindentation mechanical properties (*H* and *E*) in YSZ coatings obtained by SPS. However, a recent paper by Wang et al [9] about nanostructured YSZ coatings obtained by APS clearly showed this bimodality in the mechanical properties evaluated by nanoindentation technique. Thus, these authors proved that the elastic modulus and hardness of nanostructured YSZ coating exhibited bimodal distribution, while the conventional (microstructured) YSZ coating did not show this behaviour. In addition, an estimate of the elastic modulus on the basis of the different microstructures (unmolten and molten zones) comprising the coating layer was successfully tested.

The reason of the strong differences observed in both, hardness and elastic modulus in the different zones comprising the coatings addressed in the present work are basically due to the own microstructure of these zones. Thus as it can be observed in figure 5, unmolten or partially molten zones are made up of partially sintered nanoparticles giving rise to poor interparticle bond. On contrary, molten particles lead to stronger cohesion in the arrangement of nanoparticles improving the mechanical properties. In this sense, mechanical properties such as H and specially E, evaluated by nanoindentation can be considered a good fingerprint of the type of micriostructure developed in the deposit during the SPS process.

Conclusions

YSZ suspension was successfully deposited by SPS. A 2^k experimental with a middle point design was used in order to change the spraying parameters. All coatings show

bimodal microstructure with fully melted areas and non-melted areas where the nanostructure is exhibited.

The coating obtained using middle point parameters presented the most homogeneous microstructure. Some problems appeared when measuring hardness with a microindentator, which can be solved by using a nanoindentator. The nanoindentator shows that the two well distinguished zones throughout the coatings display different hardness and elastic modulus. Molten zones exhibited higher values of hardness and elastic modulus than these of the unmolten zones. In addition, the mechanical properties of the overall coating could be estimated from the average value between the mechanical properties of the two zones. Thus, nanoindentation has been proved to be a powerful tool to achieve a suitable mechanical characterisation of the thin layers obtained in SPS coatings.

Acknowledgments

This work has been supported by the Spanish Ministry of Science and Innovation (project MAT2009-14144-C03) and the Caixa Castelló-Bancaixa foundation (ref. E-2011-05).

References

1. L. Lima, B. R. Marple. Therm. Spary. Technol 16[1] (2007) 40-63
2. D. Chen, E. H. Jordan, M Gell. Therm. Spray. Technol. 18[3] (2009) 421-425
3. R. S. Lima, B. R. Marple. Mater. Sci. Eng. A 485 (2008) 182-193
4. P. Fauchais, G. Montavon, R. S. Lima, B. R. Marple. J. Phys. D: Appl. Phys. 44 [9] (2011) 093001
5. A. Killinger, R. Gadow, G. Mauer, A. Guignard, R. Vassen, D. Stöver. J. Therm. Spray Technol. 20 [4] (2011) 677-685
6. H. Kassner, R. Siegert, D. Hathiramani, R. Vassen, D. Stoever. Therm. Spray Technol. 17 [1] (2008) 115-123
7. E. Rayón, V. Bonache, M.d. Salvador, J.J. Roa, E. Sánchez. Surf. Coat. Technol. 205 (2011) 4192-4197
8. R. Vert, D. Chicot, C. Dublanche-Tixier, E. Meillot, A. Vardelle, G. Mariaux. Surf. Coat. Technol. 205 (2010) 999-1003
9. L. Wang, Y. Wang, X. G. Sun, J. Q. He, Z. Y. Pan, C. H. Wang. Vacuum 86 [8] (2012) 1174-1185
10. E. Lugscheider, K. Bozkin, S. Barwulf, A. Etzkorn. Surf. Coat. Technol. 138 (2001) 9-13
11. K.D. Bouzakis, A. Lontos, N. Michailidis, O. Knotek, E. Lugcheider, K. Bobzin. Surf. Coat. Technol 163 (2003) 75-80
12. K. Gross, S. Saber-Samandari. Surf. Coat. Technol. 203 (2009) 2995-2999
13. E. Rayón, V. Bonache, M.d. Salvador, E. Bannier, E. Sánchez, A. Denoirjean, H. Ageorges. Surf. Coat. Technol. 206 (2012) 2655-2660
14. C. Pierlot, L. Pawlowski, M. Bigan and P. Chagnon. Surf. Coat. Technol. 202 (2008) 4483-4490

15. S. Kozerski, L. Latka, L. Pawlowski, F. Cernuschi, F. Petit, C. Pierlot, H. Podlesak, J. P. Laval. J. Eur. Ceram. Soc. 31 (2011) 2089-2098
16. S. Kozerski, L. Pawlowski, R. Jaworski, F. Roudet, F. Petit. Surf. Coat. Technol. 204 (2010) 1380-1387
17. G. Di Girolamo, F. Marra, C. Blasi, E. Serra, T. Valente. Ceram. Int. 37 [7] (2011) 2711-2717
18. M. Karger, R. Vaßen, D. Stöver. Sur. Coat. Technol. 206[1] (2011) 16-23
19. G. Witz, V. Shklower, W. Steurer. J. Am. Ceram. Soc. 91 [8] (2007) 1-6

Tables

Table I. Main spraying parameters

Sample	**Power (kW)**	**Ar flow rate (slpm*)**	**H_2 flow rate (slpm)**	**Distance (mm)**	**Linear speed (mm/s)**	**Injection pressure (bar)**	**Feed suspension flow rate (g/min)**	**T_{max} (ºC)**
1	40	40	5	40	250	1.5	13	456
2						3.5	20	421
3					300	2	16	338
4					350	1.5	13	315
5						3.5	20	309

*slpm: standard litre per minute

Table II. Microhardness of YSZ coatings

Sample	**2**	**3**	**4**	**5**
Microhardness (GPa)	2.8±0.7	3.9±0.9	1.8±0.5	1.8±0.4

Figure captions

Figure 1. Cross-sectional FEG-SEM image of the as-sprayed YSZ barrier. The nanoindentation tests were performed on molten areas (m-I) and fine particle microstructure (m-II) in order to test flat surfaces (sample1)

Figure 2. Cross-section FEG_SEM micrograph of the SPS coatings

Figure 3. Surface FEG_SEM micrograph of the SPS coatings

Figure 4. XRD pattern of sample 3

Figure 5. Cross-section FEG-SEM image of the as-sprayed YSZ after polishing procedure showing the bimodal microstructure of molten areas (m-I) and fine particles (m-II), the normal cracks (N-cracks) and parallel cracks (P-cracks) respect to the substrate (sample 2)

Figure 6. Nanoindentation hardness curves for the analyzed microstructures shown in figure 2

Figure 7. Nanoindentation Young's Modulus curves for the analyzed microstructures shown in figure 2

Figures

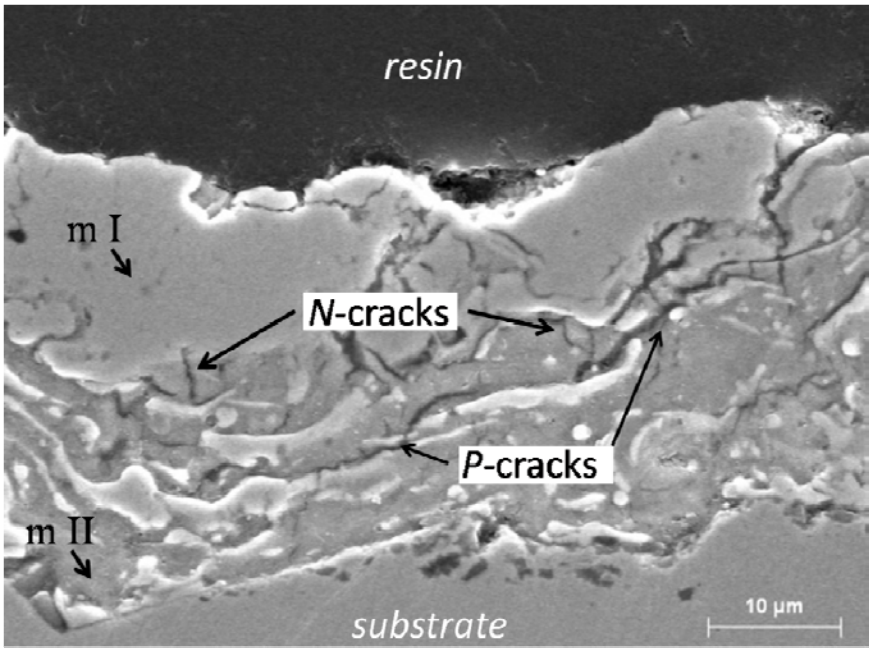

Figure 1

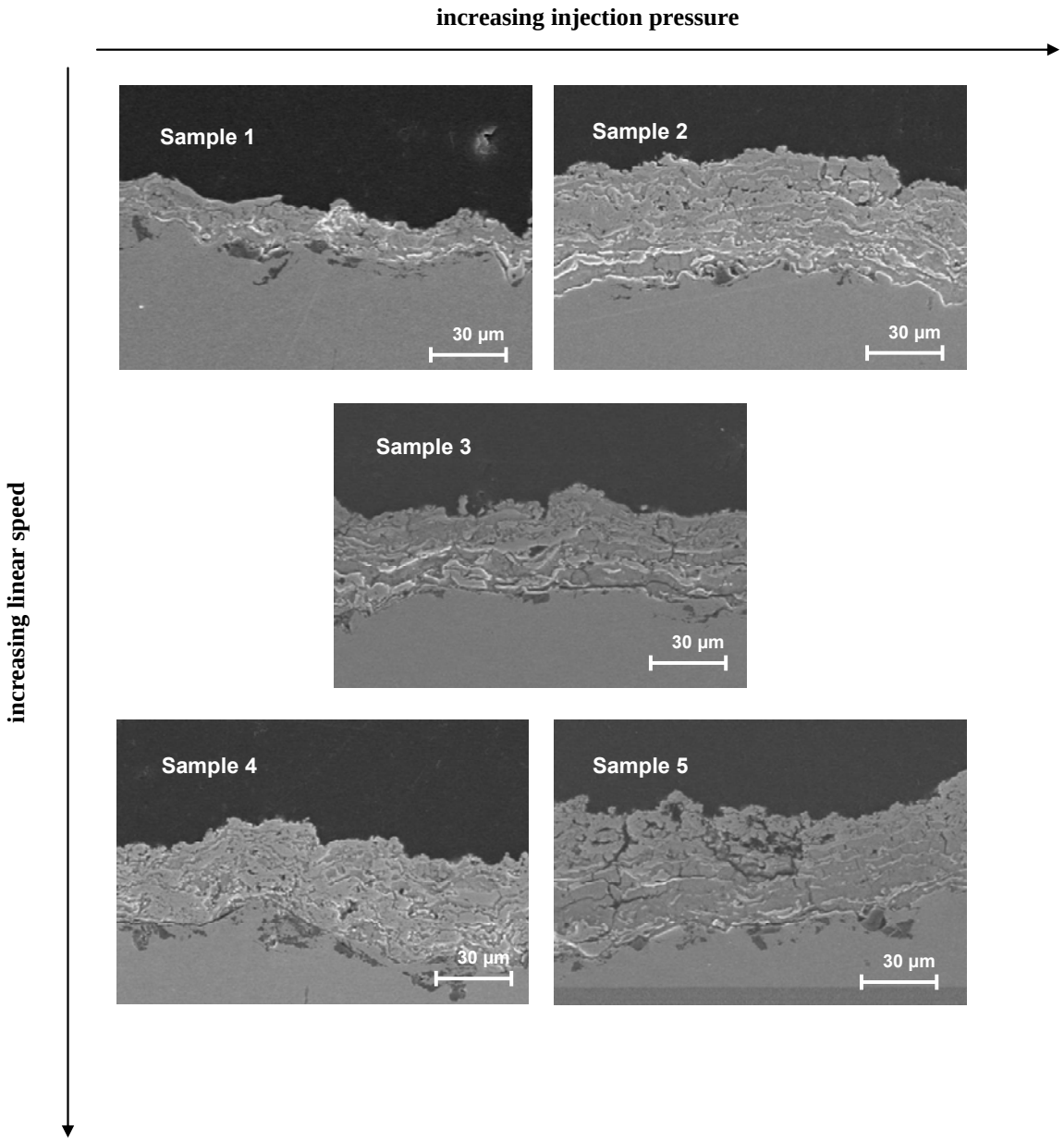
increasing injection pressure
increasing linear speed
Sample 1
30 µm
Sample 2
30 µm
Sample 3
30 µm
Sample 4
30 µm
Sample 5
30 µm

Figure 2

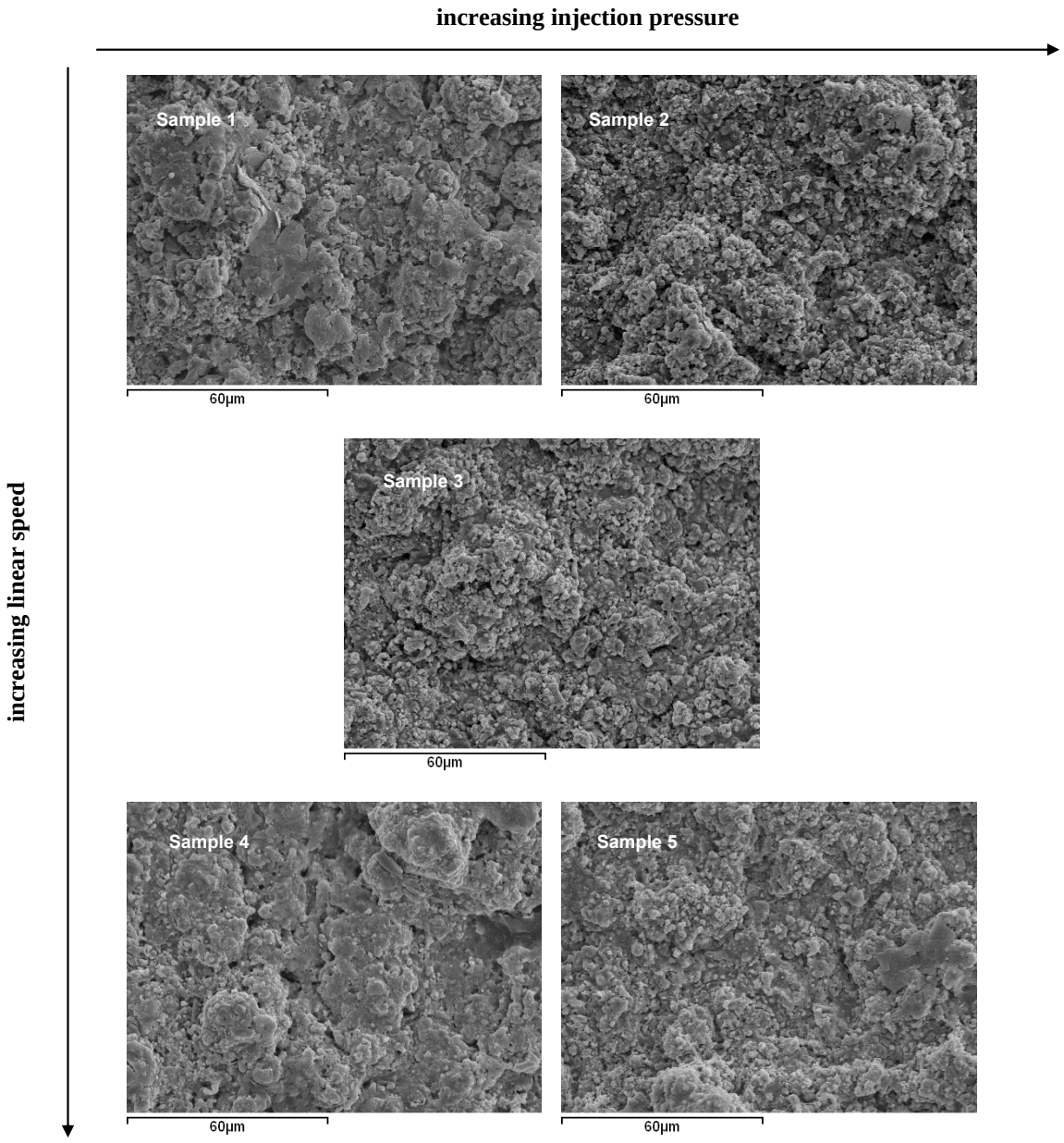
increasing injection pressure
increasing linear speed
Sample 1
Sample 2
Sample 3
Sample 4
Sample 5
60µm
60µm
60µm
60µm
60µm

Figure 3

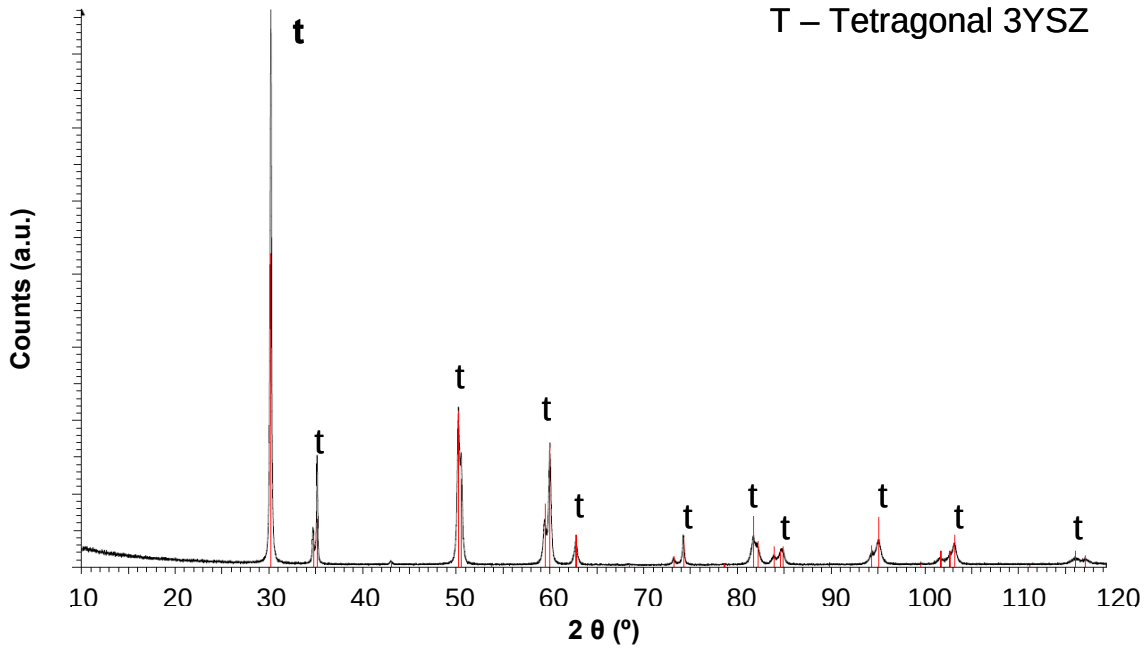

Figure 4

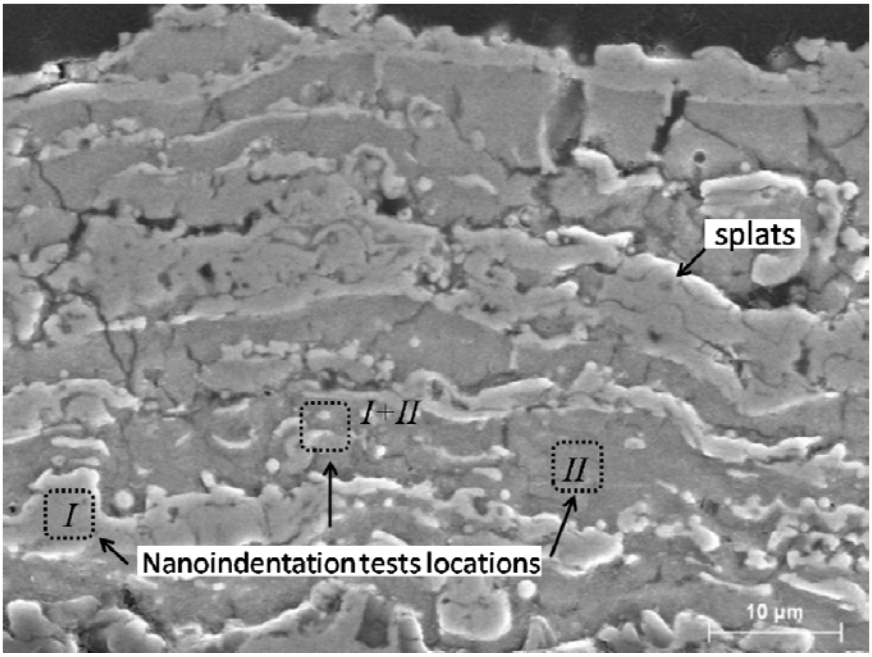

Figure 5

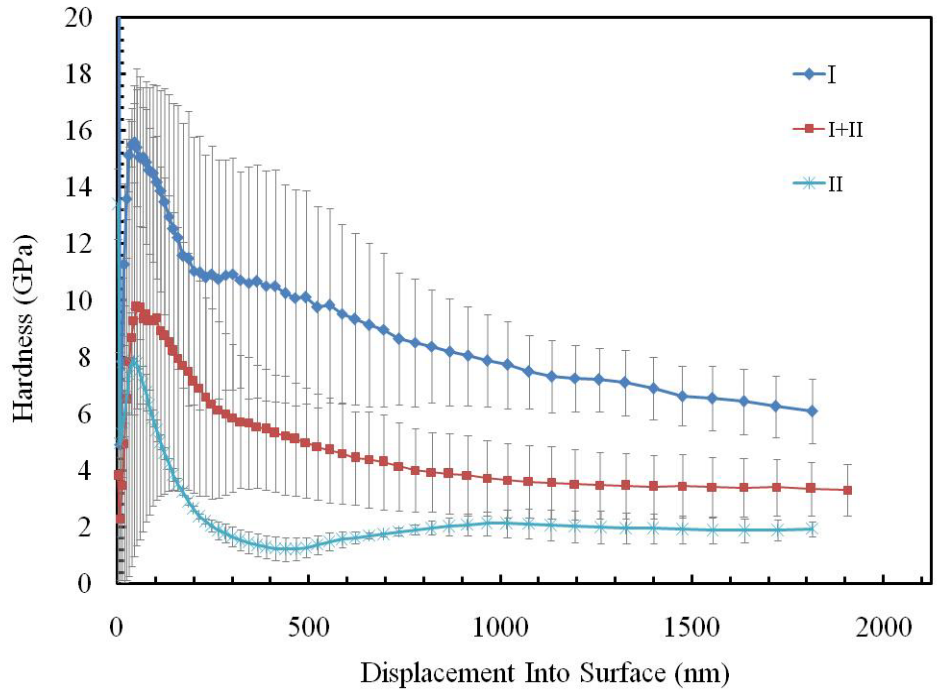

Figure 6

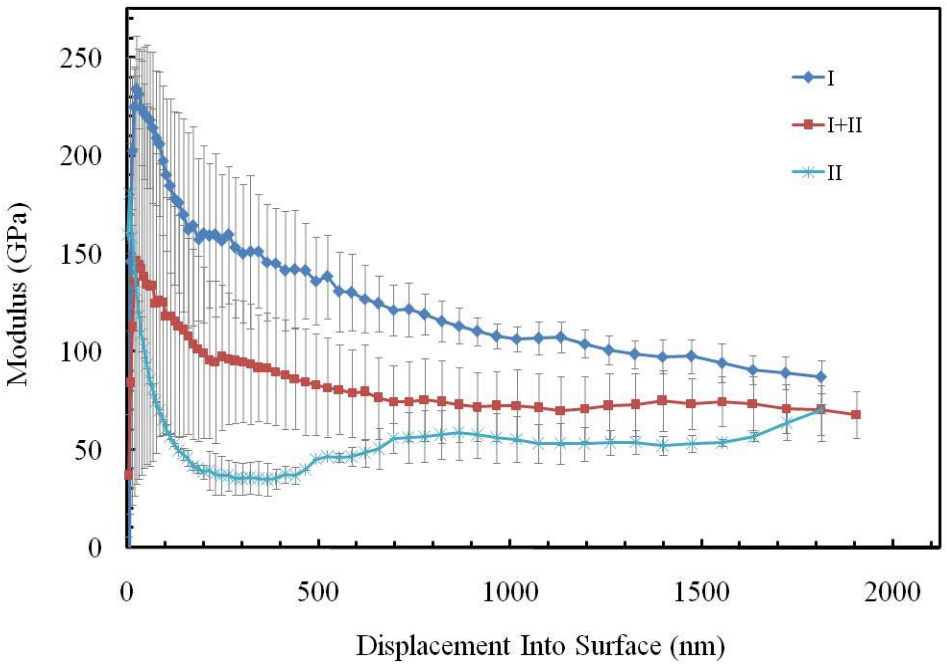

Figure 7